ON THE INCORPORATION OF SPATIAL INFORMATION TO ENDMEMBER IDENTIFICATION ALGORITHMS WITHOUT THE PURE PIXEL ASSUMPTION

Gabriel Martín, Javier Plaza and Antonio Plaza

Hyperspectral Computing Laboratory
Department of Technology of Computers and Communications
University of Extremadura, Escuela Politécnica de Cáceres
Avda. de la Universidad s/n, 10071 Caceres, Spain
{gamahefpi, jplaza, aplaza}@unex.es

ABSTRACT

Spectral unmixing is a commonly used technique in hyperspectral data exploitation. It expresses the measured spectral signature of each pixel in the data as a combination of spectrally pure constituent spectra, called *endmembers*, and a set of correspondent fractions, or *abundances* that indicate the proportion of each endmember present in the mixture. Over the last years, several algorithms have been developed for automatic endmember identification by assuming the presence of at least one pure spectral signature for each distinct material. However, this assumption often does not hold in practice due to spatial resolution, mixing phenomena, and other considerations. In this paper, we investigate if spatial information can assist the endmember searching process conducted by algorithms that do not assume the presence of pure pixels in the hyperspectral data. For this purpose, we use recently developed spatial pre-processing techniques that do not require modifications in the subsequent endmember identification process, conducted in this work using minimum volume enclosing algorithms. Our experimental results, conducted using both simulated and real hyperspectral data sets, reveal that spatial information can be beneficial to guide the endmember identification process when pure pixels are not assumed to be present in the hyperspectral data.

Index Terms— Spectral unmixing, endmember identification, spatial preprocessing, minimum enclosing volume.

1. INTRODUCTION

Most of spectral signatures (pixel vectors) collected in remotely sensed hyperspectral images are mixtures of pure components called *endmembers* [1], [2]. Linear spectral unmixing aims at representing each mixed pixel in the image as a linear combination of the endmembers and their *fraction abundances*. Let us denote the reflectance at channel i from a given pixel of the original hyperspectral image as:

$$y_i = \sum_{j=1}^{p} \rho_{ij}\alpha_j + w_i, \tag{1}$$

where ρ_{ij} denotes the reflectance of endmember j at wavelength λ_i, α_j denotes the abundance of endmember j at the considered pixel, and p is the number of endmembers. The abundances are generally subject to the abundance sum-to-one constraint (ASC) and the abundance non-negativity constraint (ANC):

$$\sum_{j=1}^{p} \alpha_j = 1, \quad \alpha_j \geq 0, \quad j = 1, \ldots, p. \tag{2}$$

Let $\mathbf{y}_i$ be an $B \times 1$ vector, where B is the total number of bands, and $\mathbf{m}_j \equiv [\rho_{1j}, \rho_{2j}, \ldots, \rho_{Bj}]^T$ be the spectral signature of the jth endmember. Expression (1) can then be written in compact matrix form as:

$$\mathbf{Y} = \mathbf{MS} + \mathbf{W}, \tag{3}$$

where $\mathbf{Y}$ is a hyperspectral image made up of n pixel vectors in total, defined as $\mathbf{Y} \equiv [\mathbf{y}_1, \ldots, \mathbf{y}_n] \in \mathbb{R}^{B \times n}$. $\mathbf{M} \equiv [\mathbf{m}_1, \mathbf{m}_2, \ldots, \mathbf{m}_p] \in \mathbb{R}^{B \times p}$ is a matrix containing the signatures of the endmembers present in the pixel. $\mathbf{S} \equiv [\boldsymbol{\alpha}_1, \ldots, \boldsymbol{\alpha}_n] \in \mathbb{R}^{p \times n}$ is a matrix containing the fractional abundances, and $\mathbf{W} \in \mathbb{R}^{B \times n}$ models additive noise.

Several techniques have been adopted in the literature to estimate the matrix of endmembers $\mathbf{M}$ by assuming the presence of pure pixels in the original hyperspectral data. Examples include the orthogonal subspace projection (OSP) algorithm [3], the N-FINDR algorithm [4], or vertex component analysis (VCA) [5]. However, this assumption may not hold in real hyperspectral data sets due to spatial resolution, mixing phenomena, and other considerations [1]. In order to deal with this issue, several methods have been developed that do not assume the presence of pure signatures in the dataset. These methods aim at generating *virtual* endmembers (not necessarily present in the set comprised by input data samples). Among these techniques, minimum volume enclosing solutions have found success in the recent literature. Craig's seminal work [6] established the concepts regarding the algorithms of minimum volume type. Among representative algorithms in this category we can list (among several others) the minimum volume constrained nonnegative matrix factorization method (MVC-NMF) [7], the minimum volume simplex analysis (MVSA) algorithm [8], the convex analysis-based minimum volume enclosing simplex (MVES) algorithm [9], or the simplex identification via split augmented Lagrangian (SISAL) algorithm [10]. These methods aim at estimating the endmember matrix $\mathbf{M}$ by minimizing the volume of the simplex defined by its columns and containing the observed spectral vectors.

In this work, our purpose is to evaluate if spatial information can be used to assist in the identification of the endmember matrix $\mathbf{M}$ using minimum volume concepts. Our introspection is that spatial information may assist in the generation of endmembers which are more similar to real spectral signatures present in the data and partially overcome the problem of *false endmembers* which is generally

978-1-4577-2201-1/11/$26.00 ©2011 IEEE

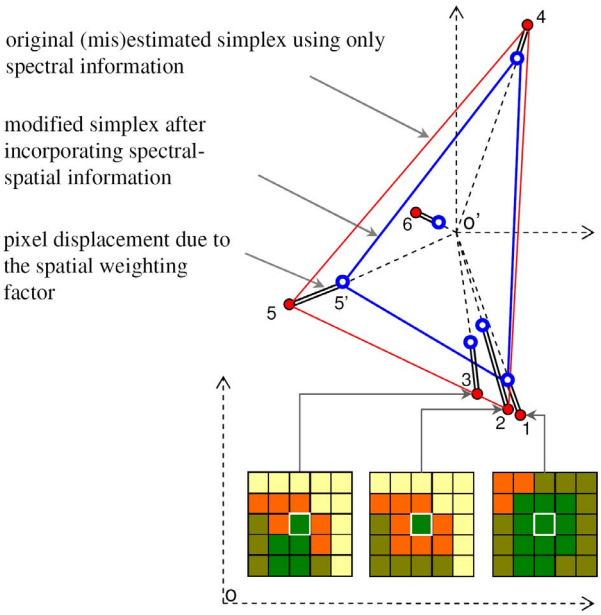

Fig. 1. Geometric interpretation of the spatial pre-processing (SPP) method.

associated to algorithms working under the minimum volume enclosure regime. The remainder of the paper is structured as follows. Section 2 describes two spatial pre-processing methods used in this work to include spatial information in the endmember identification process. In section 3 we describe the two considered minimum volume algorithms for endmember identification (MVSA and SISAL). Sections 4 and 5 respectively describe our experimental results with simulated and real hyperspectral data sets. Section 6 concludes with some remarks and hints at plausible future research lines.

2. SPATIAL PRE-PROCESSING METHODS

In this work, we use two recently proposed strategies: spatial pre-processing (SPP) [11] and region-based SPP (RBSPP) [12], as pre-processing modules prior to endmember identification:

- The SPP modifies the original simplex taking into account the spatial arrangement of the pixels. The correction is performed so that pixels located in spatially homogenous areas (e.g., the pixel labeled as '1' in Fig. 1) are expected to have a smaller displacement with regards to their original location in the data cloud than pure pixels surrounded by spectrally distinct substances (e.g., the pixels labeled as '2' and '3' in Fig. 1).
- The RBSPP uses a spectral clustering and a region detection procedure to select the regions that are more pure in spectral terms, discarding from the simplex the pixels in those regions that are composed by mixtures and retaining only the pixels that are located in spatially homogeneous regions.

3. ENDMEMBER IDENTIFICATION ALGORITHMS

The two considered endmember identification algorithms, MVSA and SISAL, implement a robust version of the minimum volume concept. The robustness is introduced by allowing the ANC to be violated. These violations are weighted using a soft constraint given by the hinge loss function ($\text{hinge}(x) = 0$ if $x \geq 0$ and $-x$ if $x < 0$). After reducing the dimensionality of the input data from B to $p-1$, MVSA/SISAL aim at solving the following optimization problem:

$$\widehat{\mathbf{Q}} = \arg\max_{\mathbf{Q}} \log(|\det(\mathbf{Q})|) - \lambda \mathbf{1}_p^T \text{hinge}(\mathbf{Q}\mathbf{Y})\mathbf{1}_n \quad (4)$$

$$\text{s.t.:} \quad \mathbf{1}_p^T \mathbf{Q} = \mathbf{q}_m, \quad (5)$$

where $\mathbf{Q} \equiv \mathbf{M}^{-1}$, $\mathbf{1}_p$ and $\mathbf{1}_n$ are column vectors of ones of sizes p and n (n stands for the number of spectral vectors), respectively, $\mathbf{q}_m \equiv \mathbf{1}_p^T \mathbf{Y}_p^{-1}$ with $\mathbf{Y}_p$ being any set of linearly independent spectral vectors taken from the hyperspectral data set $\mathbf{Y}$, and λ is a regularization parameter. Here, maximizing $\log(|\det(\mathbf{Q})|)$ is equivalent to minimizing the volume of the simplex defined by selected endmembers, $V(\mathbf{M})$.

4. EXPERIMENT WITH SYNTHETIC IMAGES

4.1. Construction of Synthetic Scenes

A database of five 100×100-pixel synthetic hyperspectral scenes has been created using fractals to generate distinct spatial patterns often found in nature. In this work, we used fractals to simulate linear mixtures of a set of endmember signatures randomly selected from a spectral library compiled by the U.S. Geological Survey (USGS)[1] and made up of a total of 420 signatures. Fig. 2 shows the five fractal images used to construct simulated scenes in this work, while Fig. 3 describes the procedure adopted to generate one of the synthetic images used in the simulations. As shown by Fig. 3, the original fractal is divided into a number of clusters using the k-means algorithm [13]. The abundance proportions in the regions associated to each cluster have been set so that pixels closer to the border of the region are more heavily mixed, while the pixels located at the center of the region are more spectrally pure in nature. In other words, all the simulated pixels inside a region are mixed, and the simulated image does not contain completely pure pixels. This increases the complexity of the unmixing problem and simulates the situation often encountered in real-world analysis scenarios, in which completely pure pixels are rarely found. For this purpose, a Gaussian filter is applied where the width of the Gaussian is carefully adjusted according to the width of each region. Zero-mean Gaussian noise was added to the synthetic scenes[2] in different signal to noise ratios (SNRs) –from 30:1 to 110:1– to simulate contributions from ambient and instrumental sources, following the procedure described in [3].

4.2. Performance Metric

The performance metric used in our experiments is the spectral angle (SA) [1] between each extracted endmember and the available USGS ground-truth spectral signatures. Low SA scores mean high spectral similarity between the compared vectors (the value range of SA is $[0, 90]$ degrees). This spectral similarity measure is invariant in the multiplication of pixel vectors by constants and, consequently, is invariant before unknown multiplicative scalings that may arise due to differences in illumination and angular orientation. The SA allows us to identify the USGS signature which is most similar to each endmember by observing the minimum SA distance reported

[1] http://speclab.cr.usgs.gov/spectral.lib06

[2] http://www.umbc.edu/rssipl/people/aplaza/fractals.zip

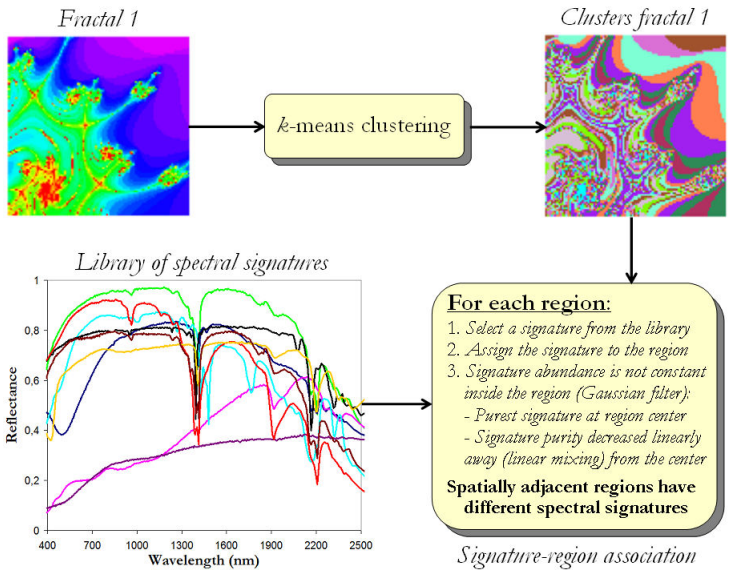

Fig. 3. Block diagram describing our procedure for generating synthetic hyperspectral images.

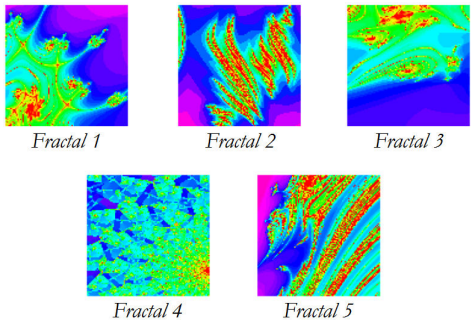

Fig. 2. Synthetic images used in experiments, where spatial patterns were generated using fractals.

for such endmember across the entire set of available USGS signatures using the following spectral similarity matching algorithm. Let us denote by $\mathbf{M} \equiv [\mathbf{m}_1, \mathbf{m}_2, \ldots, \mathbf{m}_p]$ the set of p endmembers extracted by a certain algorithm from a hyperspectral scene, and let $\mathbf{G} \equiv [\mathbf{g}_1, \mathbf{g}_2, \ldots, \mathbf{g}_q]$ denote a set of ground-truth spectral signatures. We can establish the correspondence between ground-truth endmembers in set $\mathbf{G}$ and the endmembers obtained from the image data in set $\mathbf{M}$ as follows:

1. *Initialization*. The endmembers in $\mathbf{G}$, $\mathbf{M}$ are 'unmatched.'
2. *Matching*. For each unmatched endmember in set $\mathbf{G}$, calculate the SA between such endmember and all endmembers in the set $\mathbf{M}$. Determine the pair $\{\mathbf{m}_i, \mathbf{g}_j\}$, with $1 \leq i \leq p$ and $1 \leq j \leq q$ with the minimum obtained value of $\text{SA}(\mathbf{m}_i, \mathbf{g}_j)$ after comparing all possible combinations, then label the associated endmembers, $\mathbf{m}_i$ and $\mathbf{g}_j$ as 'matched.'
3. *Iterative procedure and termination*. Each time $\{\mathbf{m}_i, \mathbf{g}_j\}$ have been 'matched', $\mathbf{m}_i$ is removed from $\mathbf{M}$ and $\mathbf{g}_j$ is removed from $\mathbf{G}$. Once these endmembers have been removed, the process is repeated from step 2 until all endmembers in set $\mathbf{G}$ have been labeled as 'matched.'.

4.3. Performance Evaluation

Before describing our experiments with simulated data, it is first important to address the parameters used for the SPP and RBSPP methods adopted for spatial pre-processing. In the case of SPP, the only input parameter is the size of the spatial neighborhood around each pixel vector (see Fig. 1), which was empirically set to a size of 5×5 pixels [11]. In the case of RBSPP, we use the well-known ISODATA algorithm [13] to obtain the initial regions, where the number of classes found by the ISODATA algorithm is automatically established by considering a minimum value $c_{min} = p$ and a maximum value $c_{max} = 2p$, being p the number of endmembers used to generate the images (fixed in our experiments to $p = 9$).

Table 1 shows the average SA scores (in degrees) between the reference USGS mineral spectra and their corresponding endmember pixels produced by several endmember identification algorithms, across the five synthetic scenes in Fig. 2. As a result, each value reported in Table 1 corresponds to the average SA obtained after processing the five considered scenes with the same SNR (five different SNR values, ranging from 30:1 to 110:1, are reported in the table). In our experiments we have considered two minimum volume enclosing algorithms without the pure pixel assumption (MVSA and SISAL). For a detailed assessment on the impact of SPP and RBSPP on endmember identification algorithms designed under the pure pixel assumption, we refer interested readers to [12].

As shown by Table 1, both MVSA and SISAL perform very accurately (low SA scores) when the SNR is high (i.e., between 70:1 and 110:1). However, when the SNR decreases to a range between 30:1 and 50:1, the algorithms can benefit from the incorporation of spatial information which removes outliers and guides the endmember identification process to more meaningful endmembers in spectral sense, as observed by the SA scores reported in Table 1. In our experiments, the SPP is generally more effective than the RBSPP, which can only improve the obtained SA values with regards to the original SISAL for the simulated scenes with SNR=30:1, and for the simulated scenes with SNR between 50:1 and 70:1 in the case of MVSA. In turn, the SPP always improved the obtained SA results.

Table 1. Average spectral angle scores (in degrees) between the USGS mineral spectra and their corresponding endmembers produced by several endmember identification algorithms across the five synthetic scenes in Fig. 2.

Algorithm	SNR=30:1	SNR=50:1	SNR=70:1	SNR=90:1	SNR=110:1
MVSA	13.908	1.365	0.130	0.028	0.024
SPP+MVSA	12.451	1.007	0.100	0.023	0.020
RBSPP+MVSA	14.323	1.114	0.110	0.029	0.254
SISAL	13.212	2.135	1.465	1.497	1.528
SPP+SISAL	9.950	0.770	0.290	0.221	0.221
RBSPP+SISAL	12.748	4.102	3.894	3.569	3.952

Table 2. Average spectral angle scores (in degrees) between the USGS mineral spectra and their corresponding endmembers produced by several endmember identification algorithms after processing the AVIRIS Cuprite scene. 2.

Algorithm	Alunite	Buddingtonite	Kaolinite	Muscovite	Average
MVSA	10.927	4.951	18.528	10.937	11.336
SPP+MVSA	9.017	5.169	11.837	7.154	8.294
RBSPP+MVSA	10.486	4.759	8.410	7.990	7.911
SISAL	10.218	5.505	13.374	8.958	9.514
SPP+SISAL	7.353	4.058	5.884	7.205	6.125
RBSPP+SISAL	11.845	4.487	8.752	7.216	8.075

5. EXPERIMENT WITH REAL HYPERSPECTRAL DATA

In this experiment we use the well-known AVIRIS Cuprite data set, available online in reflectance units[3] after atmospheric correction. The portion used in experiments corresponds to a 191×250-pixel subset of the sector labeled as f970619t01p02_r02_sc03.a.rfl in the online data. The scene comprises 224 spectral bands between 0.4 and 2.5 μm, with full width at half maximum of 10 nm and spatial resolution of 20 meters per pixel. Prior to the analysis, several bands were removed due to water absorption and low SNR in those bands, leaving a total of 192 reflectance channels to be used in the experiments. The Cuprite site is well understood mineralogically [14]. A few selected spectra from the USGS library, corresponding to representative minerals in the Cuprite mining district, are used to substantiate endmember purity.

Table 2 tabulates the SA scores (in degrees) obtained after comparing the USGS library spectra of *alunite*, *buddingtonite*, *kaolinite* and *muscovite* (present in the selected subscene), with the corresponding endmembers obtained by different algorithms from the AVIRIS Cuprite scene. Table 2 only displays the smallest SA scores of all endmembers with respect to each USGS signature for each considered algorithm. For reference, the average SA values across the five USGS signatures are also reported. In all cases, the number of endmembers to be identified was set to $p = 10$ after visual assessment of USGS mineral maps generated for the considered subscene[4]. As shown by Table 2, on average the use of SPP and RBSPP always improved the results achieved by MVSA and SISAL.

6. CONCLUSIONS AND FUTURE RESEARCH

In this paper, we have addressed the issue of how to incorporate spatial information into endmember identification algorithms designed without assuming the presence of pure pixels in the hyperspectral data. Our experimental study indicates that spatial information can provide an useful source of information to discard *outliers* (in our context, pixels which are not located in spatially homogeneous areas) and thus assist the endmember identification process, with the ultimate goal of producing more realistic spectral signatures as the final endmembers. Further experiments with additional hyperspectral scenes and endmember identification methods without the pure pixel assumption should be performed in future work in order to fully objectify our findings.

[3] http://aviris.jpl.nasa.gov/html/aviris.freedata.html

[4] http://speclab.cr.usgs.gov/cuprite95.tgif.2.2um_map.gif

7. REFERENCES

[1] N. Keshava and J. F. Mustard, "Spectral unmixing," *IEEE Signal Processing Magazine*, vol. 19, no. 1, pp. 44–57, 2002.

[2] O. Eches, N. Dobigeon, C. Mailhes, and J.-Y. Tourneret, "Bayesian estimation of linear mixtures using the normal compositional model. application to hyperspectral imagery." *IEEE Transactions on Image Processing*, vol. 19, pp. 1403–1413, 2010.

[3] J. C. Harsanyi and C.-I. Chang, "Hyperspectral image classification and dimensionality reduction: An orthogonal subspace projection," *IEEE Transactions on Geoscience and Remote Sensing*, vol. 32, no. 4, pp. 779–785.

[4] M. E. Winter, "N-FINDR: an algorithm for fast autonomous spectral end-member determination in hyperspectral data," *Proc. SPIE Image Spectrometry V*, vol. 3753, pp. 266–277, 2003.

[5] J. M. P. Nascimento and J. M. Bioucas-Dias, "Vertex component analysis: A fast algorithm to unmix hyperspectral data," *IEEE Transactions on Geoscience and Remote Sensing*, vol. 43, no. 4, pp. 898–910, 2005.

[6] M. D. Craig, "Minimum-volume transforms for remotely sensed data," *IEEE Transactions on Geoscience and Remote Sensing*, vol. 32, pp. 542–552, 1994.

[7] L. Miao and H. Qi, "Endmember extraction from highly mixed data using minimum volume constrained nonnegative matrix factorization," *IEEE Transactions on Geoscience and Remote Sensing*, vol. 45, no. 3, pp. 765–777, 2007.

[8] J. Li and J. Bioucas-Dias, "Minimum volume simplex analysis: a fast algorithm to unmix hyperspectral data," *Proc. IEEE International Geoscience and Remote sensing Symposium*, vol. 3, pp. 250–253, 2008.

[9] T.-H. Chan, C.-Y. Chi, Y.-M. Huang, and W.-K. Ma, "A convex analysis-based minimum-volume enclosing simplex algorithm for hyperspectral unmixing," *IEEE Transactions on Signal Processing*, vol. 57, pp. 4418–4432, 2009.

[10] J. Bioucas-Dias, "A variable splitting augmented lagragian approach to linear spectral unmixing," *First IEEE GRSS Workshop on Hyperspectral Image and Signal Processing-WHISPERS'2009*, 2009.

[11] M. Zortea and A. Plaza, "Spatial preprocessing for endmember extraction," *IEEE Transactions on Geoscience and Remote Sensing*, vol. 47, pp. 2679–2693, 2009.

[12] G. Martin and A. Plaza, "Region-based spatial preprocessing for endmember extraction and spectral unmixing," *IEEE Geoscience and Remote Sensing Letters, accepted for publication*, 2011.

[13] J. A. Richards and X. Jia, *Remote Sensing Digital Image Analysis: An Introduction*. Springer, 2006.

[14] R. N. Clark, G. A. Swayze, K. E. Livo, R. F. Kokaly, S. J. Sutley, J. B. Dalton, R. R. McDougal, and C. A. Gent, "Imaging spectroscopy: Earth and planetary remote sensing with the usgs tetracorder and expert systems," *Journal of Geophysical Research*, vol. 108, pp. 1–44, 2003.